

Supporting Information

Multinitrogen π -Conjugated Conductive Polymers Stabilizing Ultra-Large Interlayer Spacing in Vanadium Oxides for High-Performance Aqueous Zinc-Ion Batteries

Weijian Li,^{ab} Kaiyue Zhu,^{*ab} Weikang Jiang,^a Hanmiao Yang,^{ab} Weili Xie,^{ab} Zhengsen Wang,^a and Weishen Yang^{*ab}

[a] W. Li, K. Zhu, W. Jiang, H. Yang, W. Xie, Z. Wang, W. Yang

State Key Laboratory of Catalysis, Dalian Institute of Chemical Physics, Chinese Academy of Sciences, Dalian 116023, China, E-mail: yangws@dicp.ac.cn (W. Yang); zky218@dicp.ac.cn (K. Zhu)

[b] W. Li, K. Zhu, H. Yang, W. Xie, Z. Wang, W. Yang

University of Chinese Academy of Sciences, Beijing 100049, China

Experimental section

Synthesis

Synthesis of anhydrous α -V₂O₅:

Firstly, 1.2 g of commercial V₂O₅ and 2.4 g of H₂C₂O₄·2H₂O were added into 40 mL of deionized (DI) water under vigorous stirring at 90 °C for 5 h to form a blue solution. Secondly, 10 mL of H₂O₂ (30 wt %) was added to the solution slowly and the mixture solution was stirred for 30 min. Then, 100 mL of ethanol was added into the mixture and stirred for another 1 h. Subsequently, the formed dark-green mixture was loaded into a 200 mL autoclave with a Teflon liner and held at 170 °C for 12 h. After the hydrothermal reaction, the precipitate was collected and thoroughly washed with deionized water and ethanol and dried at 60 °C for 12 h. Finally, the dry solid was calcined in air at 450 °C for 3 h. After that, anhydrous α -V₂O₅ was obtained.

Synthesis of poly-[2,2'-Bipyridin]-5-amine (PBpyA)-intercalated V₂O₅·nH₂O xerogels (designated as PBVO):

Firstly, 0.36 g of anhydrous α -V₂O₅ (2 mmol) was dispersed in 80 mL of deionized (DI) water under vigorous stirring at indoor temperature for 10 min. Secondly, 34 mg of [2,2'-Bipyridine]-5-amine (5-NH₂-Bpy) (0.2 mmol) was added into the mixture followed by stirring the mixture for 5 h. Then, the resulting saffron yellow mixture was loaded into a 200 mL autoclave with a Teflon liner and held at 150 °C for 3 h. After the hydrothermal reaction, the precipitate was collected and thoroughly washed with deionized water and ethanol and dried at 60 °C for 12 h. After that, PBVO was obtained.

Synthesis of V₂O₅·nH₂O xerogels (designated as H-V₂O₅):

Firstly, 0.36 g of anhydrous α -V₂O₅ (2 mmol) was dispersed in 80 mL of deionized (DI) water under vigorous stirring at room temperature for 10 min. Secondly, 5 mL of H₂O₂ (30 wt %) was added into the mixture followed by stirring the mixture for 5 h. Then, the pH value of the above mixture was adjusted to \approx 3 by adding 1 M HCl solution and the mixture was stirred for 30 min. The formed mixture was loaded into a 200 mL autoclave with a Teflon liner and held at 220 °C for 24 h. After the hydrothermal reaction, the precipitate was collected and thoroughly washed with deionized water and ethanol and dried at 60 °C for 12 h. After that, H-V₂O₅ was obtained.

Synthesis of poly-[2,2'-Bipyridin]-5-amine (designated as PBpyA):

Firstly, 0.11 g of [2,2'-Bipyridine]-5-amine (5-NH₂-Bpy) (0.64 mmol) was added into 5 mL of HCl solution (1 M) and stirred in ice-water bath for 1h. Secondly, 36.5 mg of Na₂S₂O₈ (0.16 mmol) was dissolved into 1mL of deionized (DI) water and the Na₂S₂O₈ solution was added into the above mixture followed by stirring the mixture for 24 h. After the reaction, the precipitate was collected and thoroughly washed with deionized water and ethanol and dried at 60 °C for 24 h. After that, PBpyA was obtained.

Preparation of the electrode

To prepare a variety of electrodes, 60 wt% active materials, 26 wt% Super-P, and 14 wt% polyvinylidene fluoride (PVDF) were thoroughly mixed and dispersed into N-methyl pyrrolidone (NMP). The resultant slurry was then coated uniformly onto Φ14 mm stainless steel meshes with an approximately 1 mg material loading, followed by vacuum drying at 100 °C for approximately 12 h and compression at 10 MPa. (the active materials mentioned in this work include including H-V₂O₅, PBVO)

Soaking experiment

A single electrode and 3 mL of 2 M ZnSO₄ were employed in the soaking experiment. Typically, the dissolution of V-based materials tends to reach a saturation concentration. The dissolution is primarily a kinetic process, with the electrolyte volume strongly impacting the dissolution. Throughout electrochemical testing, the electrolyte volume in zinc ion cells was maintained at 150 μL. For enhanced dissolution observation, a single electrode and 3 mL of electrolyte were employed in the soaking experiment.

Electrochemical Tests

Battery cell assembly:

Electrochemical tests were carried out using CR2032-type coin cells. In a ZIB, zinc foil was used as the anode, and glass microfiber filters (Whatman Grade GF/A) were used as the separator. 2 M ZnSO₄ and 2 M Zn(OTf)₂ aqueous solution with pure water as solvent were used as the electrolytes.

Electrochemical testing:

The CR2032-type coin cells were assembled in air and tested using a LAND battery testing system (CT2001A) within a potential window of 0.2-1.6 V (vs Zn²⁺/Zn). Cyclic voltammograms

(CV) and electrochemical impedance spectroscopy (EIS) were performed in a three-electrode configuration using a PARSTAT PMC electrochemical workstation. A Zn-ring were used as reference and counter electrode, respectively. The EIS measurement was carried out under open circuit voltage (OCV) in a frequency range of 100 kHz and 0.1 Hz. The galvanostatic intermittent titration technique (GITT) was employed to determine Zn²⁺ diffusivity using a series of galvanostatic discharge pulses of 10 min at 60 mA g⁻¹, followed by a 1 h relaxation. The Zn²⁺ diffusion coefficient is calculated:

$$D_{Zn^{2+}}^{GITT} = \frac{4L^2(\Delta E_s)^2}{\pi\tau(\Delta E_t)^2}$$

where τ is the constant current pulse time; L corresponds to the Zn²⁺ diffusion length, which equals the thickness of the electrode; ΔE_s is the change of steady-state voltage during a single-step GITT experiment, and ΔE_t is the change in cell voltage at a constant current minus IR-loss during each galvanic step.

Materials Characterization

Phase and microstructure determination:

X-ray diffraction (XRD) patterns of the samples were collected using a Rigaku D/MAX-2500/PC with Cu K α radiation ($\lambda=1.54 \text{ \AA}$ at 40 kV and 200 mA). The data were recorded from 5° to 60° with an interval of 0.02° and a scan speed of 5 °/min.

Microstructure. The morphologies of the samples were captured with an FEI Quanta 200 F. Elemental mapping along with morphology were obtained by a scanning transmission electron microscope (STEM, JEM-ARM200F) equipped with an energy-dispersive X-ray spectrometer (EDS). Before measurement, the samples were fully dispersed in ethanol and then deposited on a holey carbon film on a Cu grid.

TGA study:

Thermogravimetric analysis (TGA) was performed using a Pyris Diamond TG/DTA. Specimens were placed in an Al₂O₃ crucible with a lid, and TGA data were recorded under air with a flow rate of 50 mL min⁻¹ while ramping from room temperature to 600 °C at a rate of 5 °C min⁻¹, and then cooling naturally to room temperature.

XPS study:

The surface chemical compositions and oxidation states of the elements were analyzed using a Thermofisher Escalab 250 Xi+ spectrometer with Al K α X-ray radiation ($h\nu=1486.6 \text{ eV}$). Prior

to these analyses, the cycled electrodes were washed thoroughly with DI water to remove electrolyte residue and then dried in a glove box. All the binding energies were corrected by adventitious C 1s at 284.6 eV.

FT-IR study:

Fourier-transform infrared spectroscopy (FT-IR) spectra of samples in the mode of attenuated total reflection were collected on a spectrometer Nicolet 6700, with 32 scans at a resolution of 4 cm⁻¹.

Raman spectra:

Raman spectra were acquired on a Renishaw microconfocal Raman spectrometer (NanoWizard) with 532 nm excitation.

Calculation Methods

Density Functional Theory (DFT) calculations for polymer monomer (5-NH₂-Bpy) and bipolymer (PBpyA) electrostatic potential (ESP) were performed using the Gaussian 16W software package. The structures of polymer monomer (5-NH₂-Bpy) and bipolymer (PBpyA) were optimized at the GGA-BLYP/ DNP level of theory. The molecular orbital energy levels, including the lowest unoccupied molecular orbital (LUMO) and the highest occupied molecular orbital (HOMO), and the charge population sum were analyzed at the GGA-BLYP / DNP level of theory.

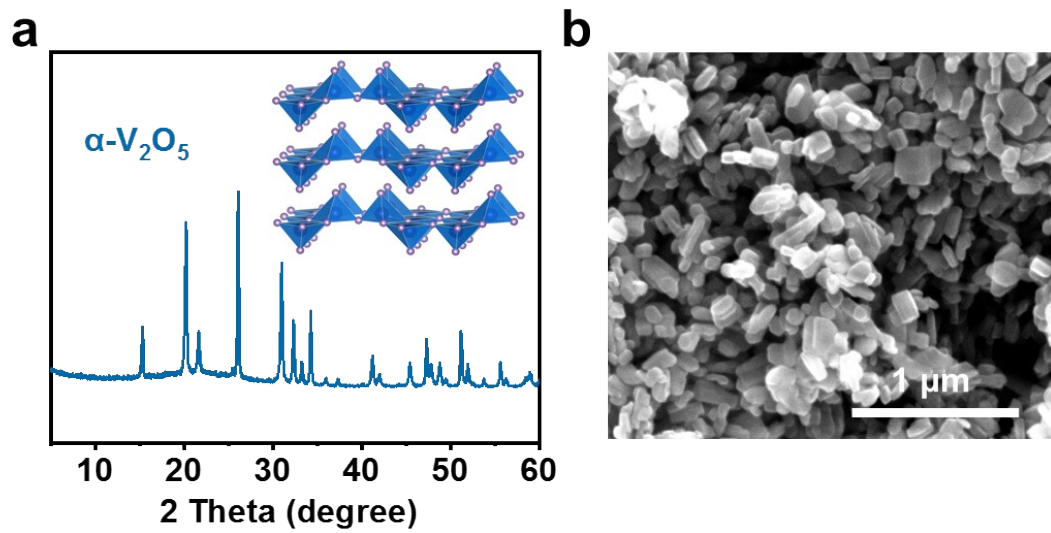


Figure S1. (a) XRD pattern of $\alpha\text{-V}_2\text{O}_5$ (inset is the corresponding crystal structure); (b) SEM image of $\alpha\text{-V}_2\text{O}_5$.

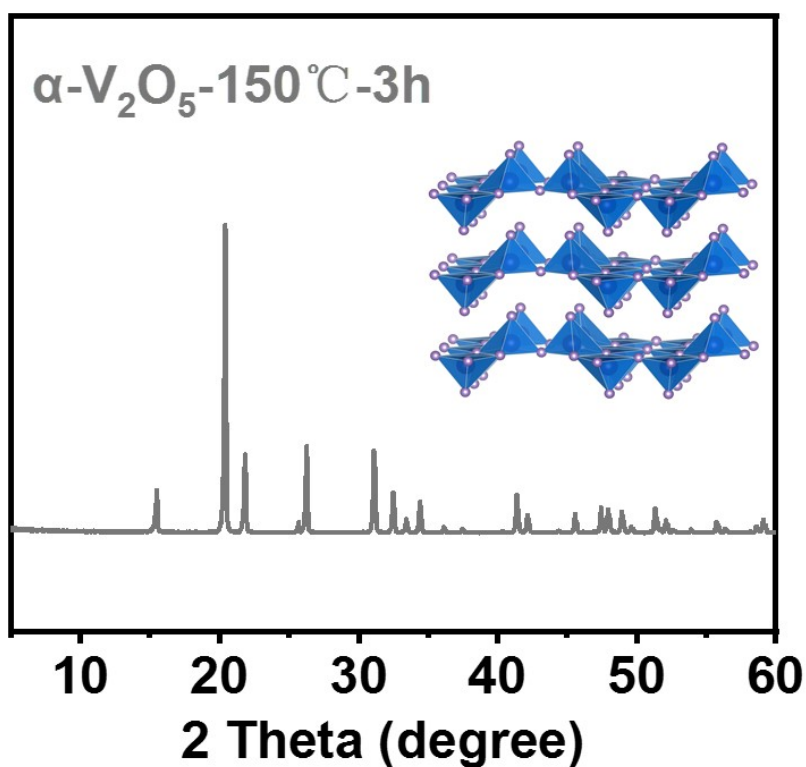


Figure S2. XRD pattern of the product from hydrothermal treatment of $\alpha\text{-V}_2\text{O}_5$ at 150°C for 3 h without polymer monomers.

In this preparation process, $\alpha\text{-V}_2\text{O}_5$ were also treated without polymer monomers under the same conditions as PBVO (150°C and 3h). As shown in Figure S2, the $\alpha\text{-V}_2\text{O}_5$ material retained its orthogonal phase and did not transform to the hydrated bilayer V_2O_5 structure. However, with addition of polymer monomers, a phase transformation was induced, resulting in the formation of the hydrated bilayer V_2O_5 (Figure 1b). This demonstrates that polymer intercalation promotes phase transition and enables synthesis under milder conditions.

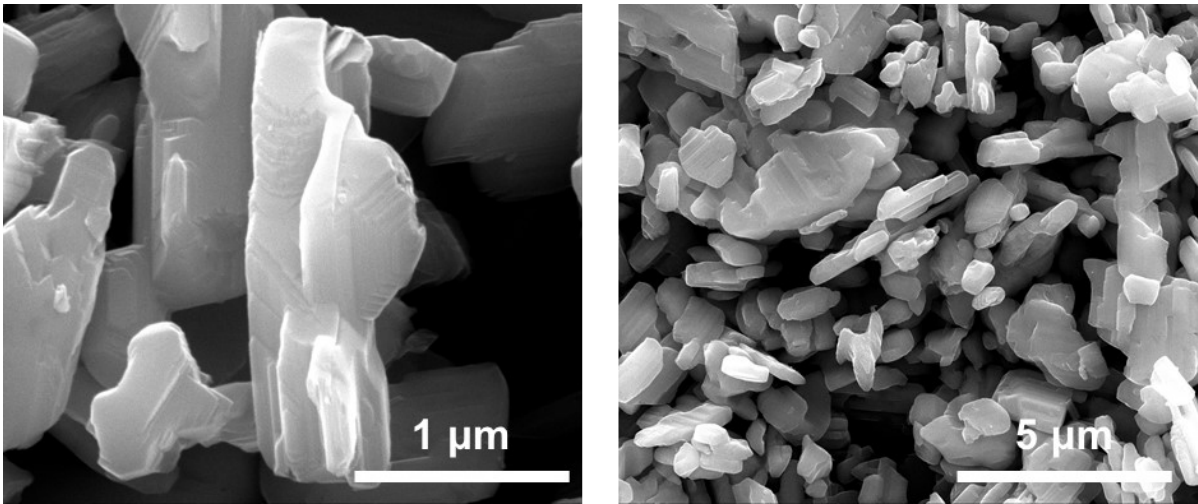


Figure S3. SEM images of the product from hydrothermal treatment of α - V_2O_5 at 150 °C for 3 h without polymer monomers.

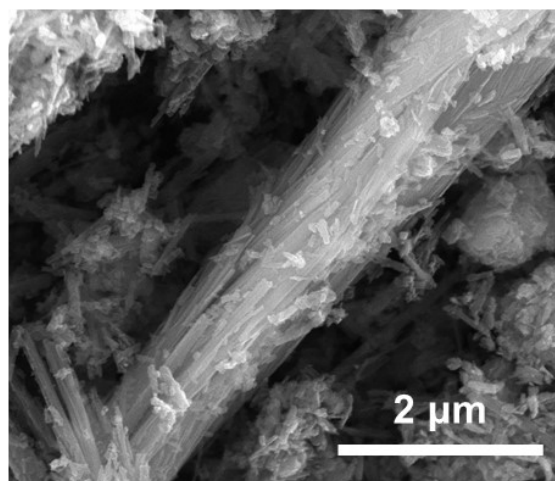
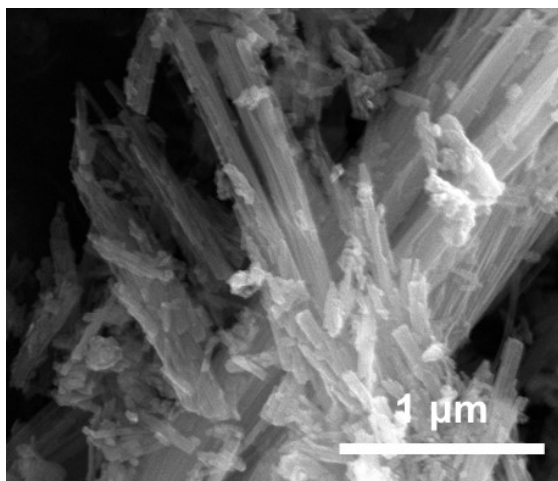


Figure S4. SEM images of H-V₂O₅ synthesized hydrothermally at 220 °C for 24 hours.

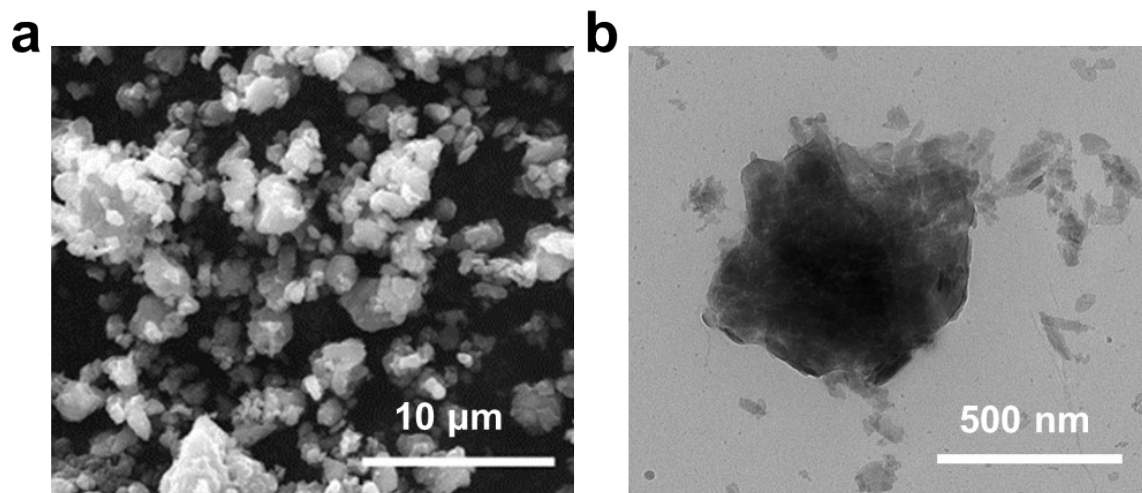


Figure S5. (a) SEM and (b) TEM images of PBVO.

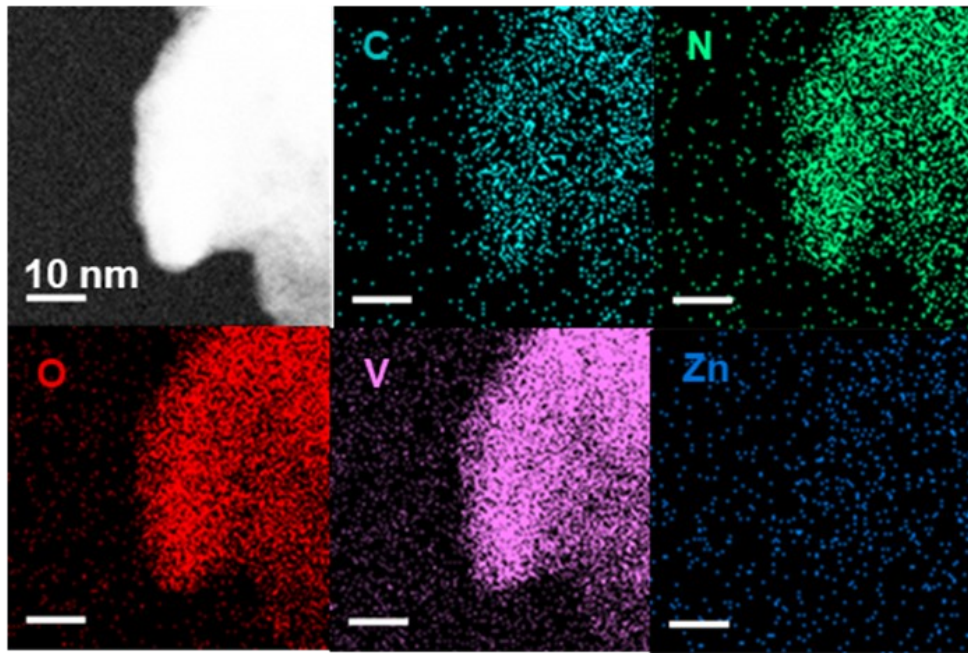


Figure S6. C, N, O, V and Zn elemental mappings of PBVO.

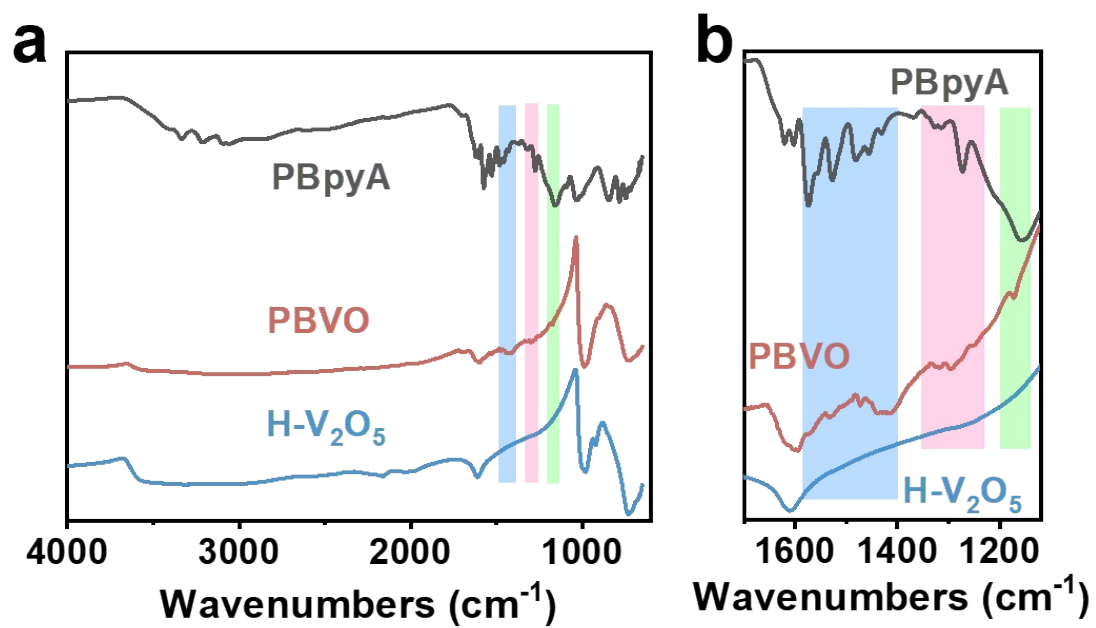


Figure S7. (a) FTIR spectra and (b) enlarged FTIR spectra for PBpyA, PBVO and H-V₂O₅.

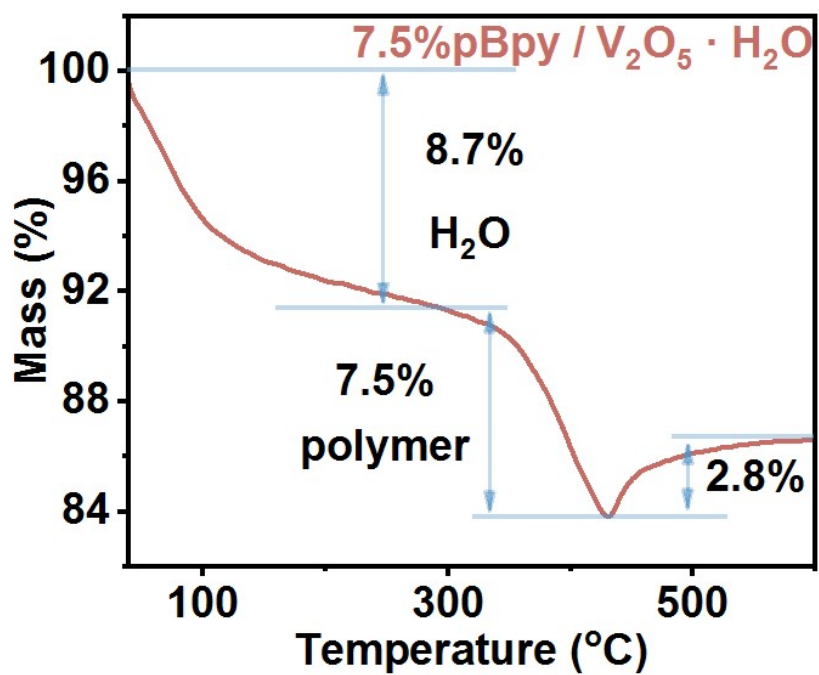


Figure S8. The TGA curve under air atmosphere of PBVO.

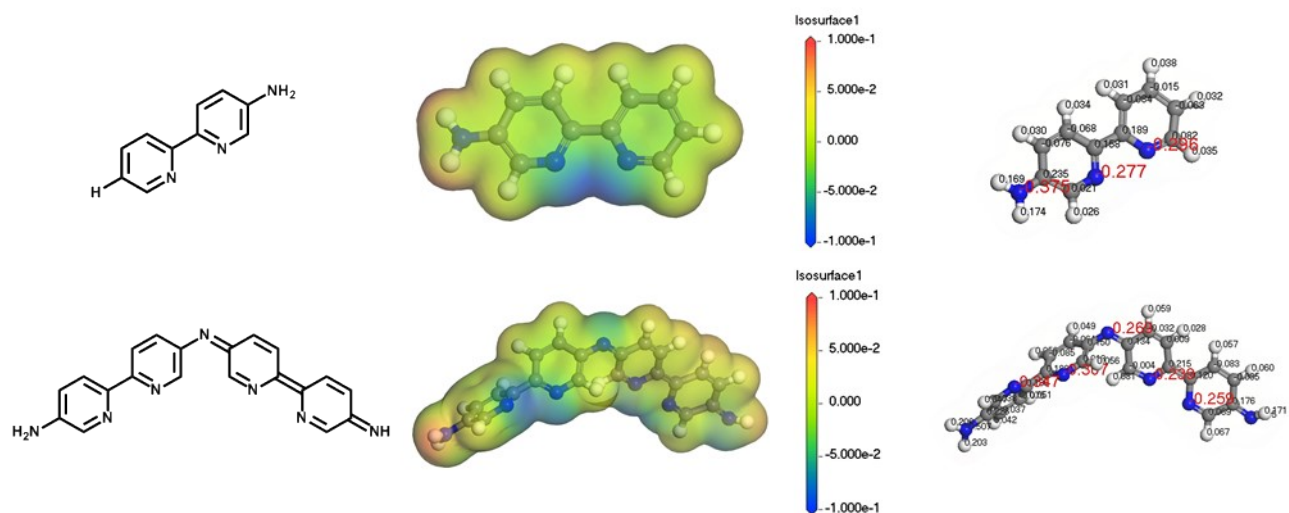


Figure S9. The molecular electrostatic potential (ESP) of polymer monomer (BpyA) and bipolymer (PBpyA).

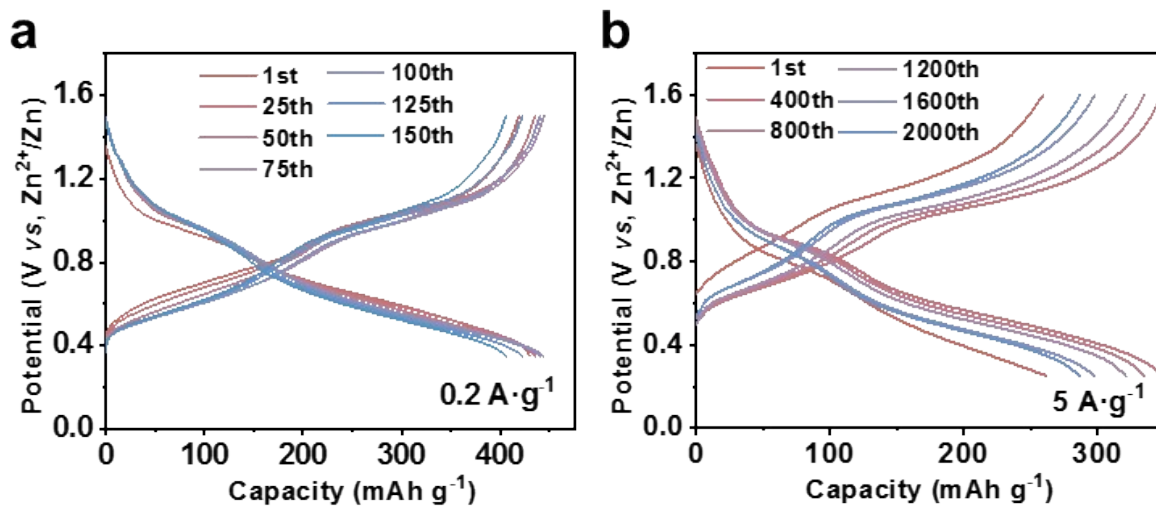


Figure S10. Galvanostatic discharge/charge profiles at (a) 0.2 A g^{-1} and (a) 5.0 A g^{-1} in a 2 M Zn(OTf)_2 aqueous electrolyte.

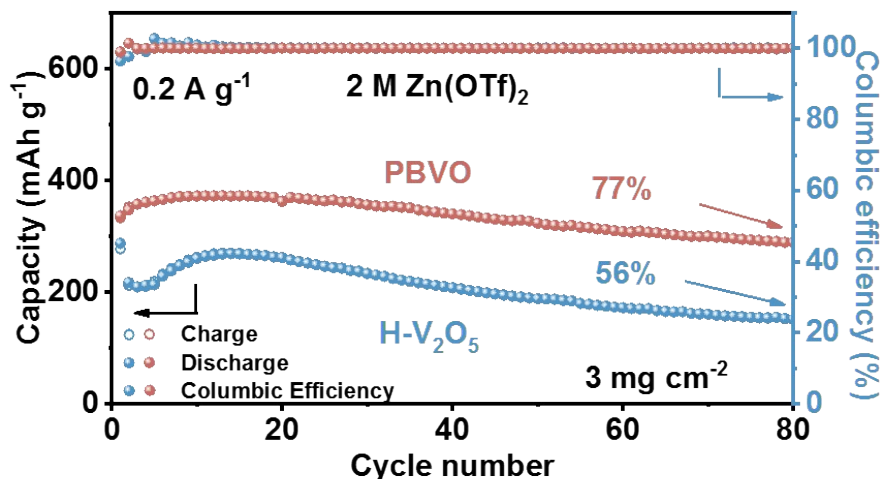


Figure S11. Cycling performances at 0.2 A g⁻¹ of PBVO and H-V₂O₅ with high mass loading (~3 mg cm⁻²).

To assess the practical application potential of PBVO, we conducted additional cycling test at 0.2 A g⁻¹ using a high active material loading of 3 mg cm⁻². As shown in Fig. S11, PBVO exhibited excellent cycling stability in 2 M Zn(OTf)₂, maintaining a specific capacity of 372.7 mAh g⁻¹ with 77 % capacity retention after 80 cycles. In contrast, H-V₂O₅ initially delivered 212.2 mAh g⁻¹, peaked at 269.7 mAh g⁻¹, and retained only 56 % of its peak capacity after 56 cycles. These results clearly demonstrate that PBVO offers significantly improved long-terms stability and performance under high mass loading of active material compared to H-V₂O₅.

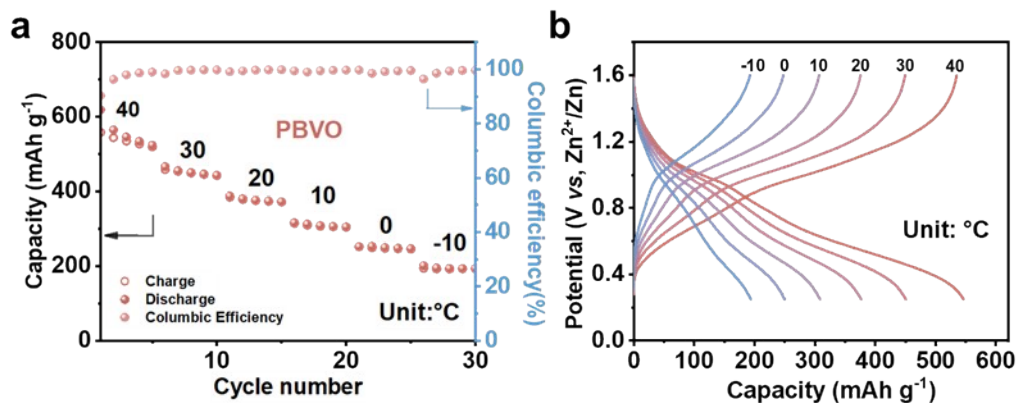


Figure S12. (a) Capacity of PBVO at temperatures ranging from 40 to -10 °C; (b) Discharge-charge curves of PBVO at various temperatures.

The temperature-dependent electrochemical performances of PBVO at current density of 0.2 A g⁻¹ in the electrolyte of 2 M Zn(OTf)₂ aqueous solution were evaluated. Tests were conducted across a temperature from 40 °C to -10 °C, in 10 °C increments. As shown in Fig. S12a and S12b, PBVO delivered discharge capacities of 546.2, 450.7, 376.6, 308.6, 249.7 and 193.6 mAh g⁻¹ at 40 °C, 30 °C, 20 °C, 10 °C, 0 °C and -10 °C, respectively. These results demonstrate that PBVO maintains good electrochemical activity across a wide temperature range, indicating strong adaptability and promising application potential at both high- and low-temperature environments.

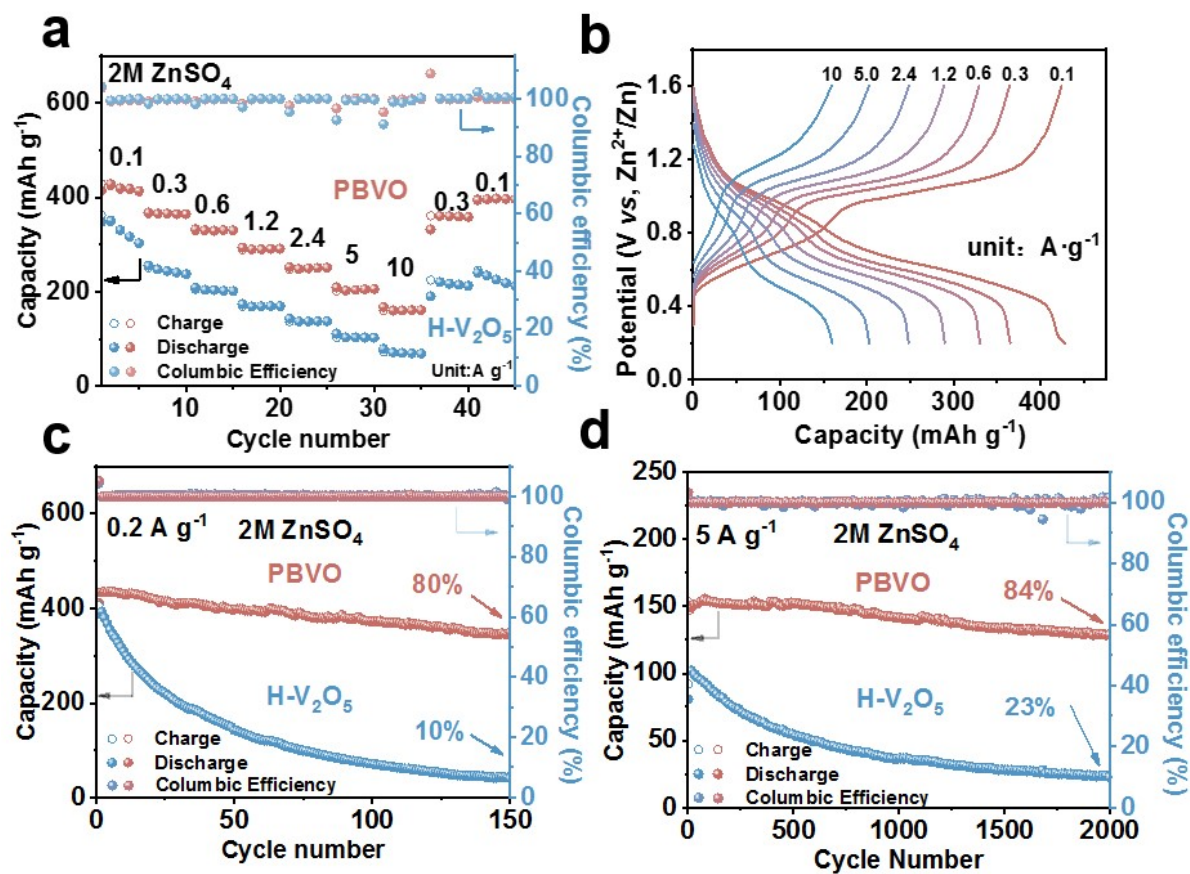


Figure S13. (a) Rate capability of PBVO in 2 M ZnSO₄ at various current densities. (b) Discharge-charge curves of PBVO at various current densities. (c) Cycling performance of PBVO at 0.2 A g⁻¹. (d) Cycling performance of PBVO and H-V₂O₅ at 5 A g⁻¹. The cathodes were tested in a coin cell-type ZIBs in 2 M ZnSO₄.

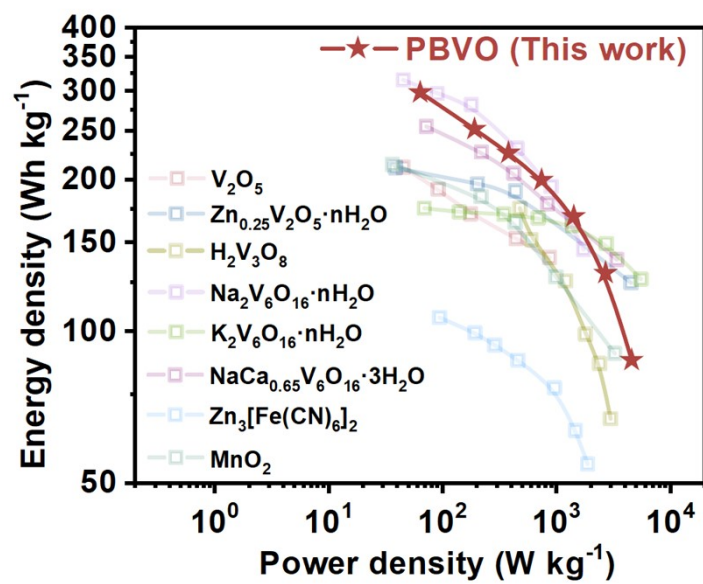


Figure S14. Ragone plot comparing with other reported ZIB cathodes. Table S1 provides a full comparison.

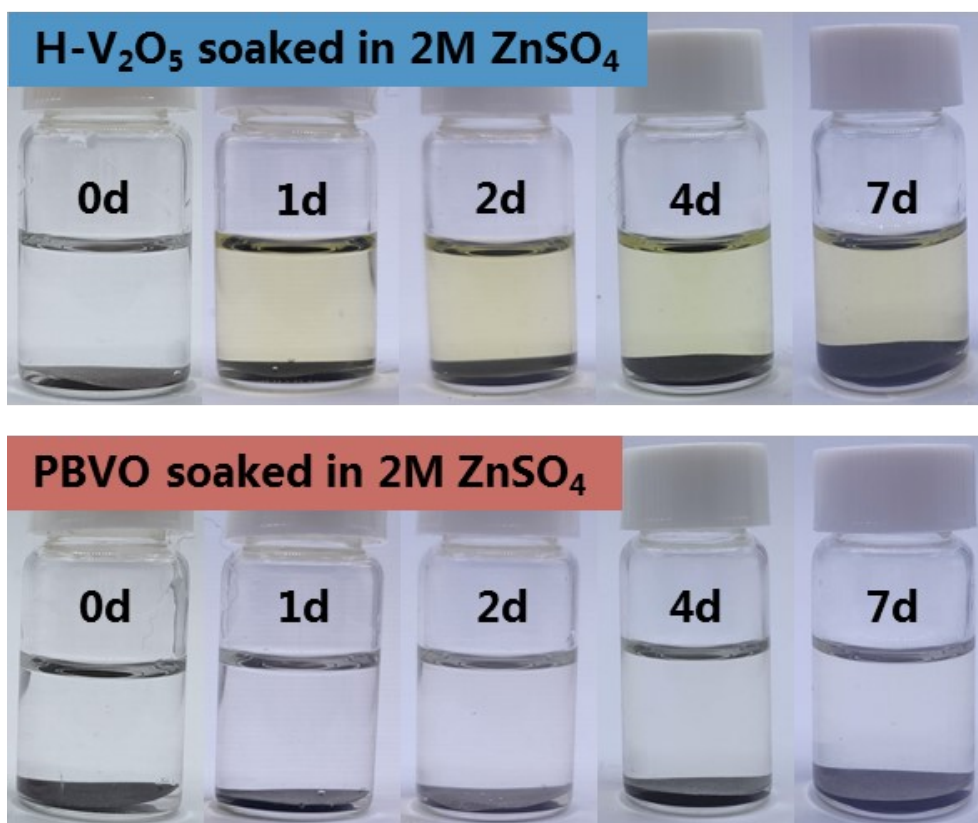


Figure S15. Optical photographs of H-V₂O₅ and PBVO electrodes soaked in 2 M ZnSO₄ for varying periods of time (0 day, 1 day, 2 days, 4 days and 7 days).

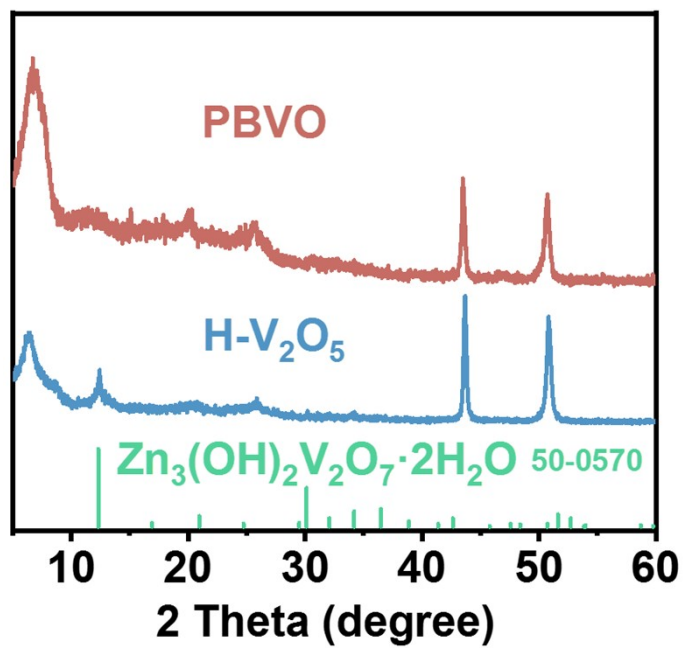


Figure S16. XRD patterns of PBVO and H-V₂O₅ cathodes after 50 cycles at 0.2 A g⁻¹ in ZIBs with an electrolyte of 2 M ZnSO₄ aqueous solution.

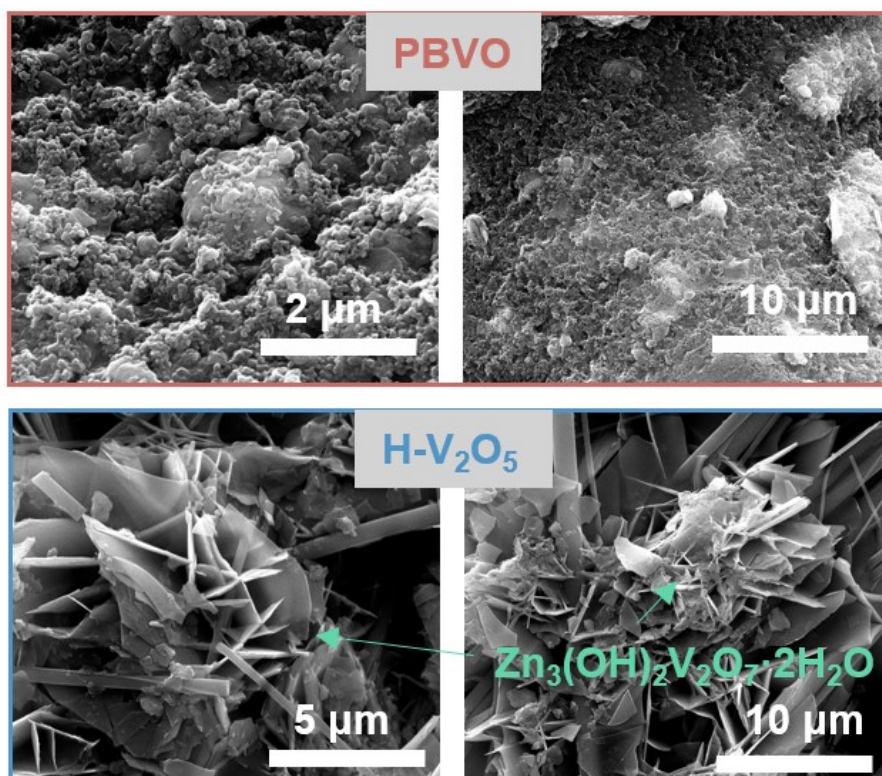


Figure S17. SEM images of PBVO and H-V₂O₅ cathodes after 50 cycles at 0.2 A g⁻¹ in ZIBs with an electrolyte of 2 M ZnSO₄ aqueous solution.

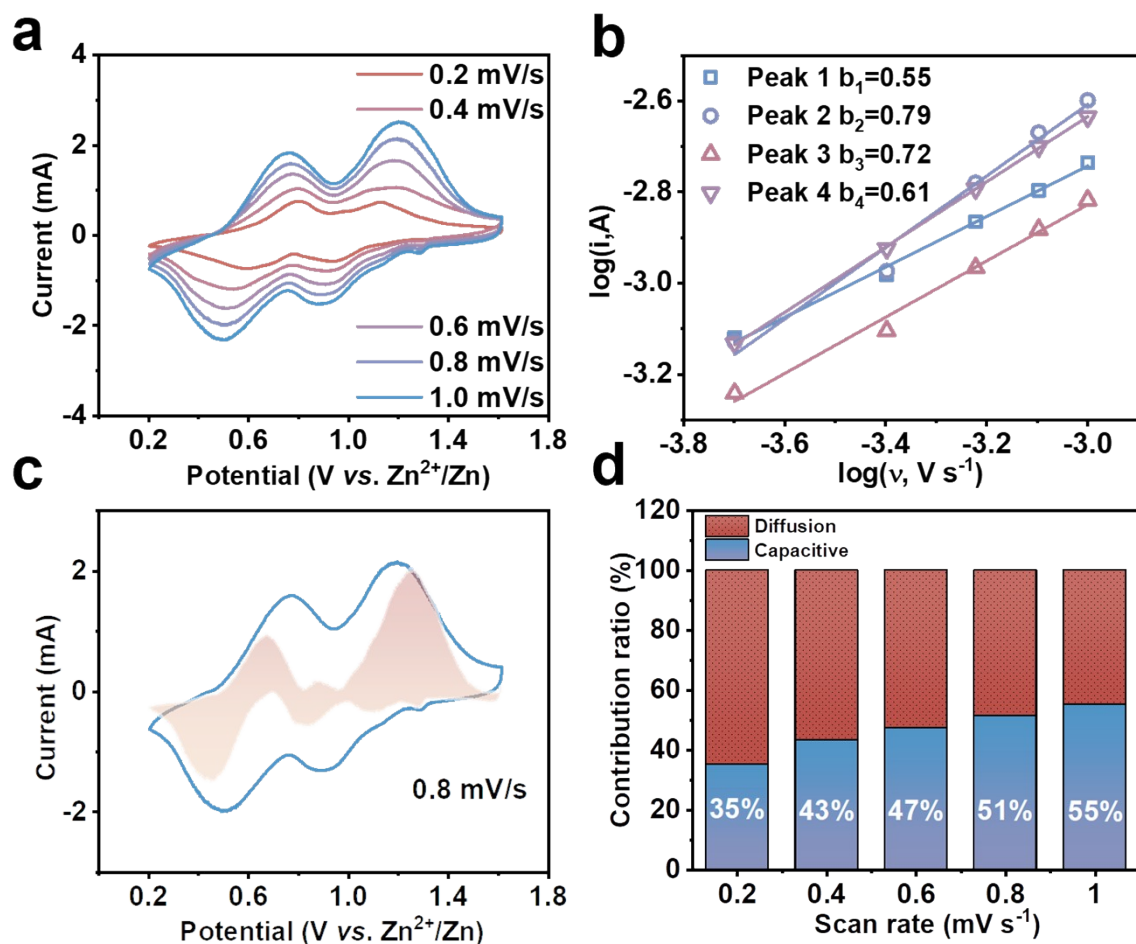


Figure S18. (a) The CV curves at various scan rates of H- V_2O_5 . (b) plots of \log (peak current) versus \log (scan rate) of H- V_2O_5 . (c) The CV curve and the capacitive contribution (pink region) at $0.8 mV s^{-1}$ of H- V_2O_5 . (d) Capacity contribution ratios at various scan rates of H- V_2O_5 .

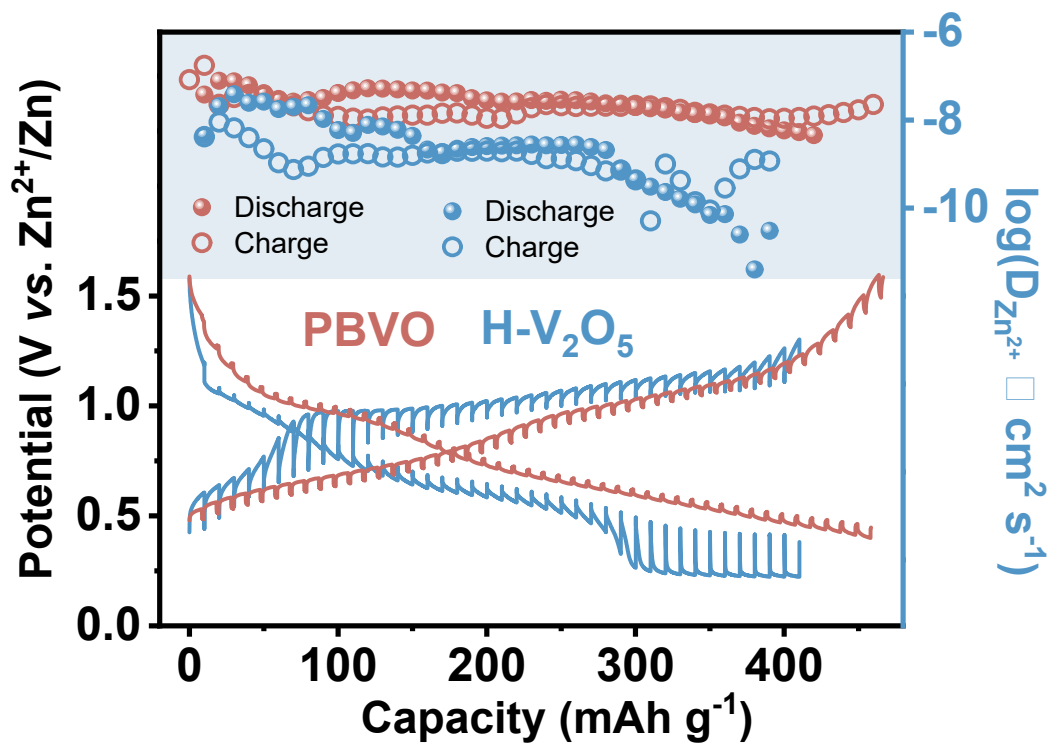


Figure S19. The Zn^{2+} diffusion coefficient of PBVO and H- V_2O_5 tested by GITT.

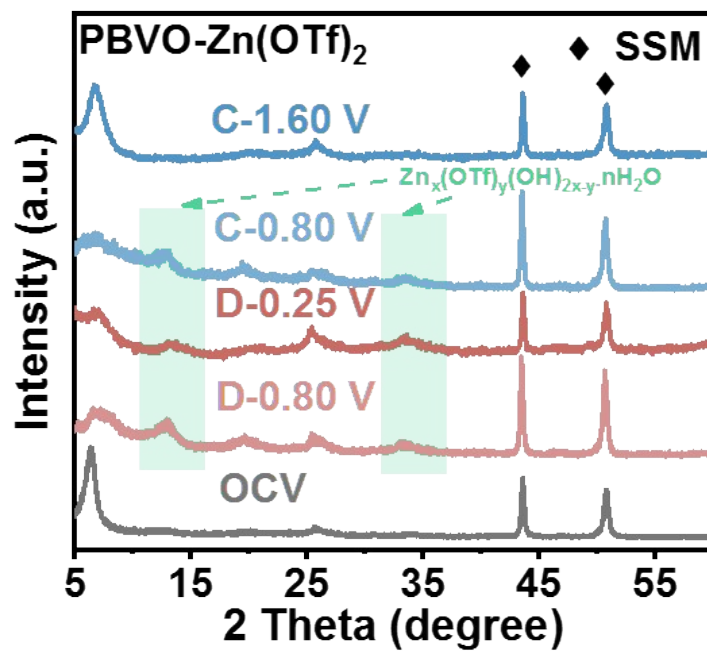


Figure S20. XRD patterns of PBVO cathodes at different SOCs in 2 M Zn(OTf)₂.

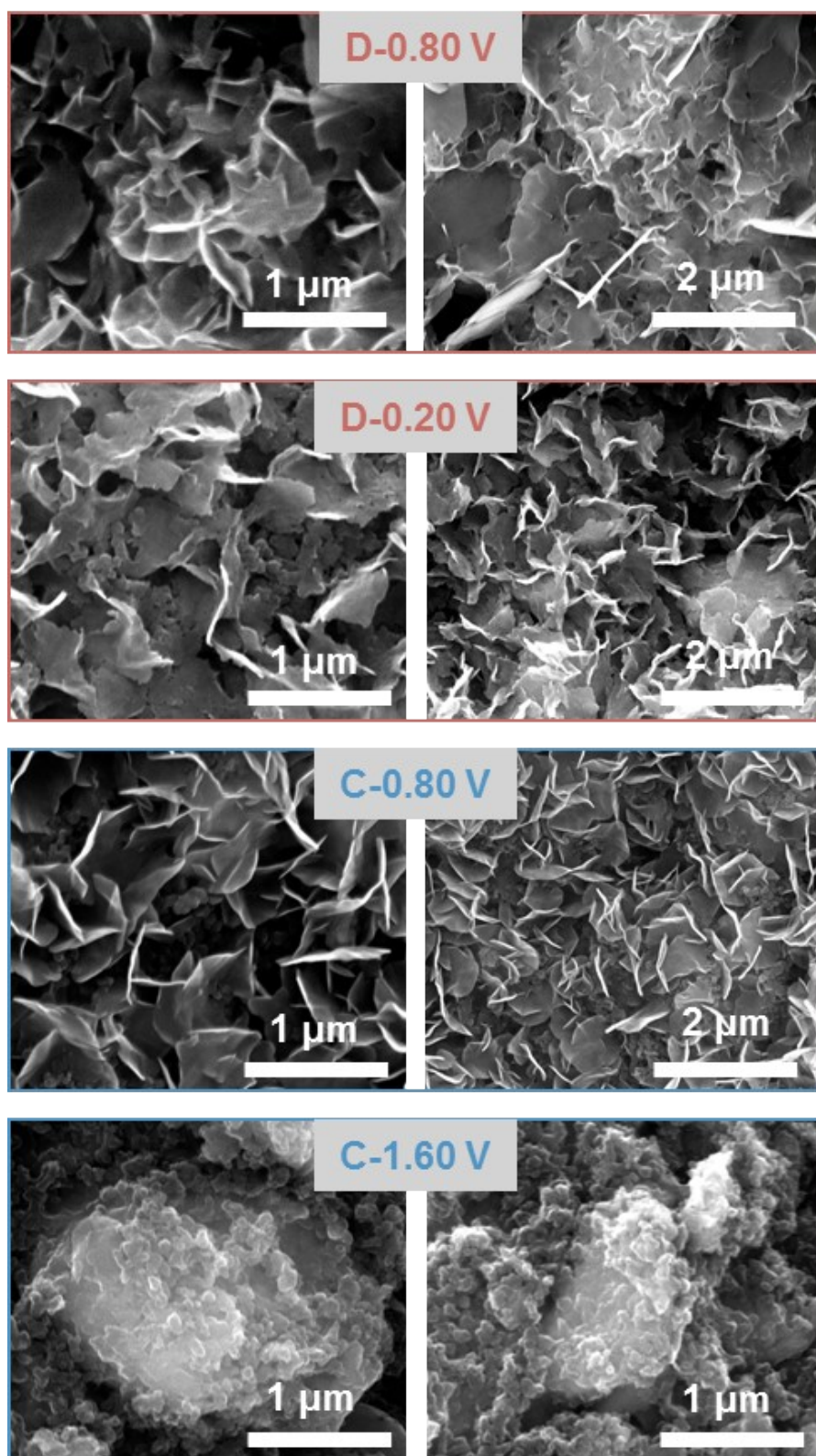


Figure S21. SEM images of PBVO cathodes at different SOC levels in 2 M $\text{Zn}(\text{OTf})_2$.

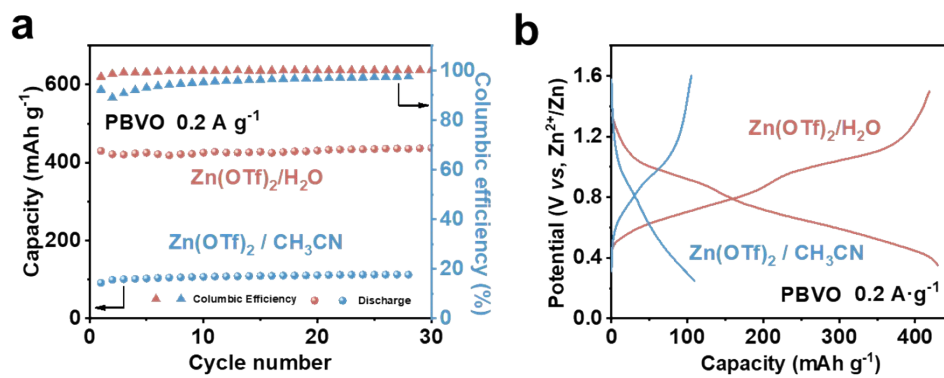


Fig. S22 (a) Cycling performances at 0.2 A g⁻¹ and (b) corresponding galvanostatic discharge/charge profiles at 15th cycle of PBVO in Zn(OTf)₂ / H₂O and Zn(OTf)₂ / CH₃CN.

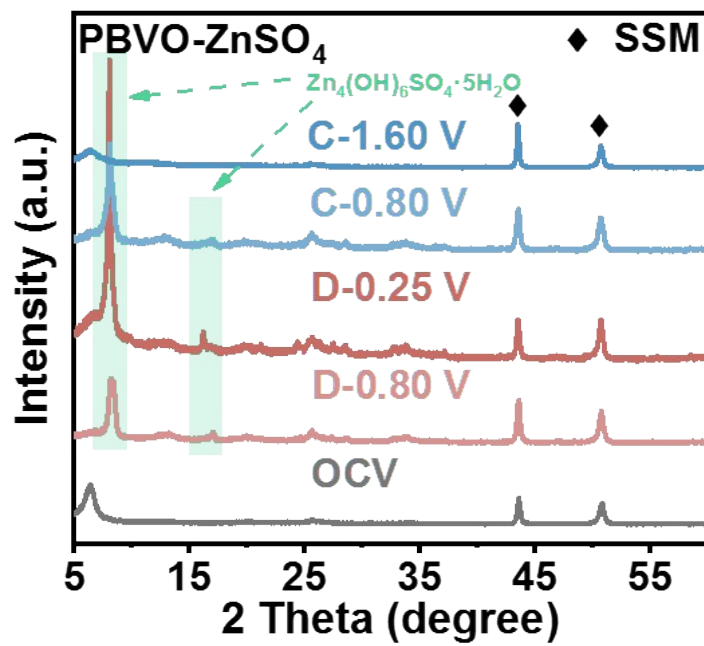


Figure S23. XRD patterns of PBVO cathodes at different SOCs in 2 M ZnSO₄.

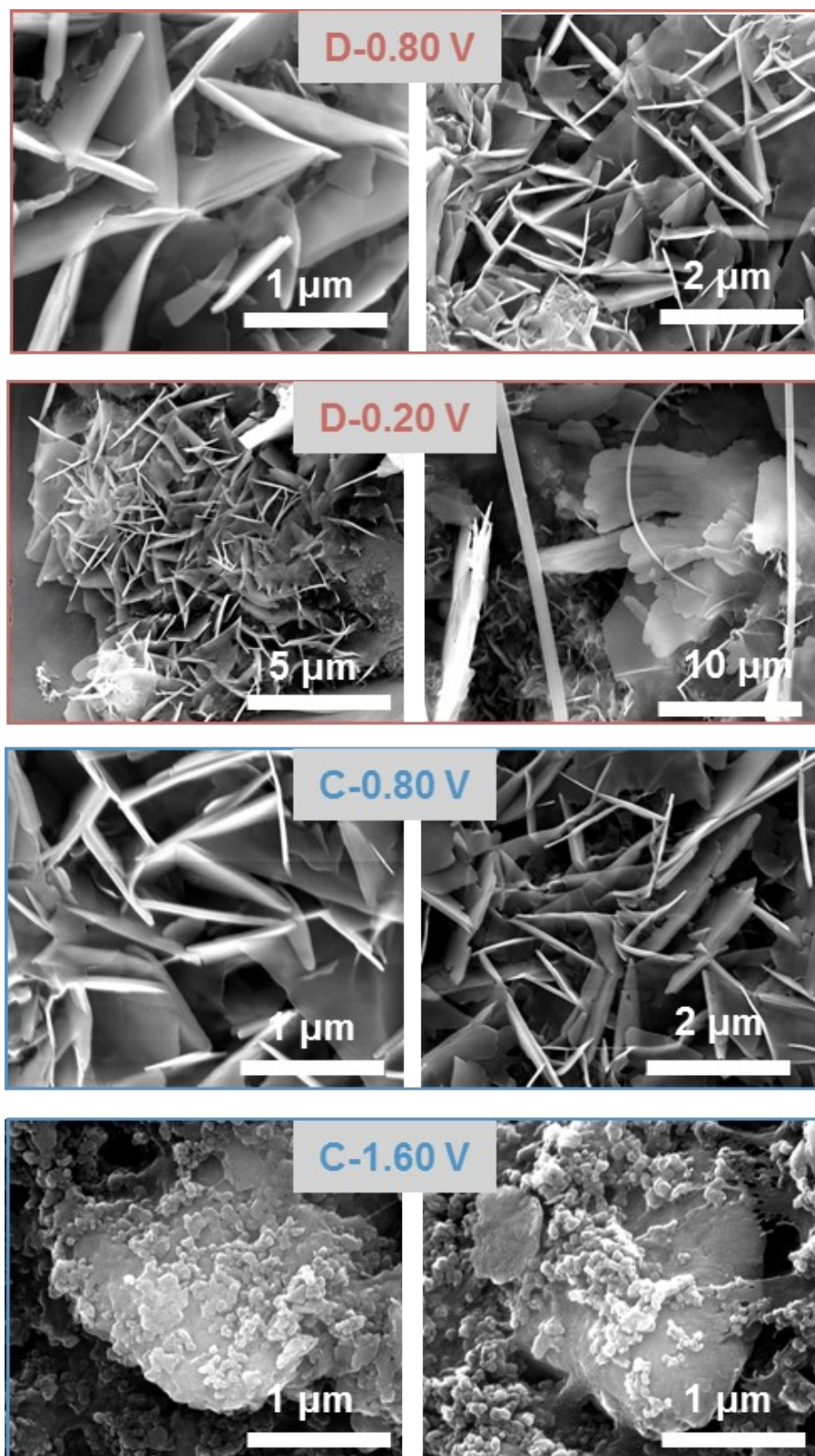


Figure S24. SEM images of PBVO cathodes at different SOCs in 2 M ZnSO_4 .

Table S1 Comparison of the electrochemical performance for the PBVO and some representative cathode materials in ZIBs.

Cathode material	Electrolyte	Specific capacity	Cycle performance	Ref.
PBVO	2 M Zn(CF ₃ SO ₃) ₂	454.6 mAh g ⁻¹ at 0.1 A g ⁻¹	429 mAh g ⁻¹ at 0.2 A g ⁻¹ 97 % retained after 150 cycles at 0.2 A g ⁻¹ 259 mAh g ⁻¹ at 5 A g ⁻¹ 84 % retained after 2000 cycles at 5 A g ⁻¹	This work
α-V₂O₅	2 M Zn(CF ₃ SO ₃) ₂	401 mAh g ⁻¹ at 0.1 A g ⁻¹	315 mAh g ⁻¹ at 2 A g ⁻¹ 73 % retained after 1000 cycles at 2 A g ⁻¹	1
Zn_{0.25}V₂O₅·nH₂O	1 M ZnSO ₄	282 mAh g ⁻¹ at 0.3 A g ⁻¹	260 mAh g ⁻¹ at 2.4 A g ⁻¹ 80 % retained after 1000 cycles at 2.4 A g ⁻¹	2
H₂V₃O₈@Graphene	3 M Zn(CF ₃ SO ₃) ₂	394 mAh g ⁻¹ at 0.1 A g ⁻¹	270 mAh g ⁻¹ at 6 A g ⁻¹ 87 % retained after 1000 cycles at 6 A g ⁻¹	3
Na₂V₆O₁₆·3H₂O	1 M ZnSO ₄	361 mAh g ⁻¹ at 0.1 A g ⁻¹	150 mAh g ⁻¹ at 14.4 A g ⁻¹ 80 % retained after 1000 cycles at 14.4 A g ⁻¹	4
K₂V₆O₁₆·3H₂O	1 M ZnSO ₄	230 mAh g ⁻¹ at 0.1 A g ⁻¹	188 mAh g ⁻¹ at 5 A g ⁻¹ 82 % retained after 500 cycles at 6 A g ⁻¹	5
NaCa_{0.6}V₆O₁₆·3H₂O	3 M Zn(CF ₃ SO ₃) ₂	347 mAh g ⁻¹ at 0.1 A g ⁻¹	231 mAh g ⁻¹ at 2 A g ⁻¹ 94 % retained after 2000 cycles at 2 A g ⁻¹ 189 mAh g ⁻¹ at 5 A g ⁻¹ 93 % retained after 2000 cycles at 5 A g ⁻¹ 83 % retained after 10000	6

Zn₃[Fe(CN)₆]₂	1 M ZnSO ₄	65.4 mAh g ⁻¹ at 0.06 A g ⁻¹	cycles at 5 A g ⁻¹	7
			53 mAh g ⁻¹ at 0.3 A g ⁻¹ 81 % retained after 100 cycles at 0.3 A g ⁻¹	
MnO₂	3 M	258 mAh g ⁻¹ at	144 mAh g ⁻¹ at 2 A g ⁻¹	8
	Zn(CF ₃ SO ₃) ₂	0.2 A g ⁻¹	94 % retained after 2000	
	+ 0.1 M Mn(CF ₃ SO ₃) ₂		cycles at 2 A g ⁻¹	

Table S2 V concentration (by ICP-OES) in 2 M ZnSO₄ aqueous electrolytes after 7 days of immersion with PBVO and H-V₂O₅.

Cathode material	V concentration (mg/L)	V concentration (mmol/L)
PBVO	0.087	0.180
H-V₂O₅	0.307	0.603

Reference

- 1 P. Hu, T. Zhu, J. Ma, C. Cai, G. Hu, X. Wang, Z. Liu, L. Zhou, L. Mai, *Chem. Commun.* 2019, **55**, 8486-8489.
- 2 D. Kundu, B. D. Adams, V. Duffort, S. H. Vajargah, L. F. Nazar, *Nat. Energy* 2016, **1**, 16119.
- 3 Q. Pang, C. Sun, Y. Yu, K. Zhao, Z. Zhang, P. M. Voyles, G. Chen, Y. Wei, X. Wang, *Adv. Energy Mater.* 2018, **8**, 1800144.
- 4 V. Soundharrajan, B. Sambandam, S. Kim, M. H. Alfaruqi, D. Y. Putro, J. Jo, S. Kim, V. Mathew, Y. K. Sun, J. Kim, *Nano Lett.* 2018, **18**, 2402-2410.
- 5 B. Sambandam, V. Soundharrajan, S. Kim, M. H. Alfaruqi, J. Jo, S. Kim, V. Mathew, Y.-k. Sun, J. Kim, *J. Mater. Chem. A* 2018, **6**, 15530-15539.
- 6 K. Zhu, T. Wu, K. Huang, *Adv. Energy Mater.* 2019, **9**, 1901968.
- 7 L. Zhang, L. Chen, X. Zhou, Z. Liu, *Adv. Energy Mater.* 2014, **5**, 1400930.
- 8 N. Zhang, F. Cheng, J. Liu, L. Wang, X. Long, X. Liu, F. Li, J. Chen, *Nat. Commun.* 2017, **8**, 405.